ACS APPLIED MATERIALS & INTERFACES

RESEARCH ARTICLE

www.acsami.org

Stabilization of Gold Nanoparticle Films on Glass by Thermal Embedding

Tanya Karakouz, Ben M. Maoz, Gilad Lando, Alexander Vaskevich,* and Israel Rubinstein*

Department of Materials and Interfaces, Weizmann Institute of Science, Rehovot 76100, Israel

Supporting Information

ABSTRACT: The poor adhesion of gold nanoparticles (NPs) to glass has been a known obstacle to studies and applications of NP-based systems, such as glass/Au-NP optical devices. Here we present a simple scheme for obtaining stable localized surface plasmon resonance (LSPR) transducers based on Au NP films immobilized on silanized glass and annealed. The procedure includes high-temperature annealing of the Au NP film, leading to partial embedding in the glass substrate and stabilization of the morphology and optical properties. The method is demonstrated using citrate-stabilized Au NPs, 20 and 63 nm mean diameter, immobilized electrostatically on glass microscope cover slides precoated with an aminosilane monolayer. Partial thermal embedding of the Au NPs in the glass occurs at temperatures in the vicinity of the glass transition temperature of the substrate. Upon annealing in air the Au NPs gradually settle into the glass and become encircled by a glass rim. In situ transmission UV−vis spectroscopy carried out during the annealing in a specially designed optical oven shows three regions: The most pronounced change of the surface plasmon (SP) band shape occurs in the first ca. 15 min of annealing; this is followed by a blue-shift of the SP band maximum (up to ca. 5 h), after which a steady red-shift of the SP band is observed (up to ca. 70 h, when the experiment was terminated). The development of the SP extinction spectrum was correlated to changes in the system structure, including thermal modification of the NP film morphology and embedding in the glass. The partially embedded Au NP films pass successfully the adhesive-tape test, while their morphology and optical response are stable toward immersion in solvents, drying, and thiol self-assembly. The enhanced adhesion is attributed to the metal NP embedding and rim formation. The stabilized NP films display a refractive index sensitivity (RIS) of 34−48 nm/RIU and 0.1−0.4 abs.u./RIU in SP band shift and extinction change, respectively. The RIS can be improved significantly by electroless deposition of Au on the embedded NPs, while the system stability is maintained. The method presented provides a simple route to obtaining stable Au NP film transducers.

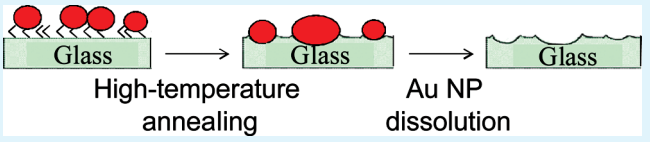

KEYWORDS: Au, adhesion, stability, high temperature, annealing, sensors, localized plasmon, LSPR

INTRODUCTION

Gold nanoparticles (NPs) support excitation of localized surface plasmons (SPs), exhibited as localized surface plasmon resonance (LSPR) extinction bands in the visible to near-infrared optical spectrum.[1] The intensity, wavelength, and shape of the SP absorption band are sensitive to the size and shape of the NPs, the interparticle distance, and the effective refractive index (RI) of the surrounding environment.[1−3] The latter enables use of Au NP films as optical transducers sensitive to alteration of the surrounding medium, such as molecular binding to the transducer surface, by monitoring the respective change in the extinction spectrum.[2−4]

Two prominent schemes used for the preparation of nanoparticulate Au films on solid supports include vapor-deposition of discontinuous Au island films,[5−15] and immobilization of prefabricated NPs from colloid solutions.[16−19] Each has its own merits, e.g., evaporation offers technical simplicity, while colloid deposition furnishes the possibility of using a wealth of NP sizes and shapes. The common substrate for Au NP based LSPR transducers of both types has been glass, providing low cost and transparency in the visible to near-IR range, useful for transmission spectroscopy. However, the poor adhesion of Au to glass frequently results in system instability, seen as morphological changes and particle coalescence upon immersion and drying,[6,20−23] affecting the optical response and complicating the preparation of recognition interfaces based on Au NP films on glass. Organic adhesion layers[24,25] may not withstand various treatments applied during interface preparation and sensing, which may result in NP detachment and aggregation.[4,20,21,26]

Efficient stabilization of the morphology and optical response of LSPR transducers can be achieved by application of ultrathin inert overlayers encapsulating the metal nanostructures.[27−30] We have published a scheme for stabilization of evaporated Au island films by coating the islands with an ultrathin (ca. 2.0 nm) sol−gel silica layer.[31]

Encapsulation ensures system stability, but the application of a overlayer lowers the sensitivity of the system to RI change because of the exponentially decaying SP evanescent field. Recently we have presented a simple, one-step procedure for obtaining strongly bonded and morphologically stable Au island films on glass substrates, showing stable optical properties under

Received: September 14, 2010
Accepted: February 21, 2011
Published: March 09, 2011

various chemical treatments. The method is based on annealing of thin evaporated Au films at temperatures close to or slightly above the glass transition temperature (T_g) of the substrate (550−600 °C).[25,32] The improved adhesion is attributed to partial embedding of the Au islands in the glass substrate accompanied by formation of a glass rim around the islands.

In the present study we use a NP embedding approach similar to that used by us for stabilizing Au island films,[25,32] i.e., annealing at temperatures in the vicinity of T_g of the glass. Previous works on Au NP embedding[33,34] included annealing at temperatures higher than T_g by ca. 200 °C. Such extensive heating frequently leads to deformation of the glass substrate, interfering with the optical measurements. Here we show that thermal embedding of Au NPs in the glass at temperatures close to T_g provides stable plasmonic transducers suitable for LSPR sensing applications.

The system studied comprised citrate-stabilized Au NPs immobilized from solution on a glass substrate modified with 3-aminopropyl trimethoxysilane (APTS). The NP film morphology was characterized by high-resolution scanning electron microscopy (HRSEM) and atomic force microscopy (AFM) imaging. Transmission UV−vis spectra were measured in situ during high-temperature annealing using a specially built optical oven, and correlated with the development of the Au film morphology. Stability of the morphology and optical response was tested using adhesive-tape test, immersion in solvents and drying, as well as alkanethiol monolayer self-assembly. The bulk refractive index sensitivity (RIS) of the Au NP films was determined by immersion in a series of methanol-chloroform solutions, showing values in the range 34 − 48 nm/RIU in SP shift and 0.1−0.4 abs.u./RIU in extinction change. Electroless deposition of Au on the stabilized Au NPs leads to enhancement of the RIS by a factor of 2−3 with no significant effect on the system stability.

EXPERIMENTAL SECTION

Chemicals. Chloroform (AR, Gadot), ethanol (Baker analyzed, J.T. Baker), methanol (anhydrous, Mallinckrodt chemicals), xylene (AR, BioLab), sulfuric acid (95−98%, BioLab), hydrogen peroxide (30%, Frutarom), 3-aminopropyl trimethoxysilane (APTS) (Aldrich), hydroxylamine hydrochloride (AR, Merck), sodium tetrachloroaurate (III) dihydrate ($NaAuCl_4 \cdot 2H_2O$) (99.99%, Alfa Aesar), trisodium citrate dihydrate (Na_3-citrate) (GR, Merck), and 1-octadecanthiol ($C_{18}SH$) (Merck) were used as received. Phosphate buffer saline (PBS) solution was prepared by 10-fold dilution of commercial reagent GIBCO D-PBS (10X)-$CaCl_2$,-$MgCl_2$ (Invitrogen) with water. Hydrogen tetrachloroaurate (III) trihydrate ($HAuCl_4 \cdot 3H_2O$) was prepared according to a known procedure.[35] Water was triply distilled. The inert gas used was household nitrogen (from liquid N_2).

Gold Nanoparticle (NP) Synthesis. Citrate-stabilized Au NPs of different dimensions were prepared according to known literature procedures.[36,37] Small Au NPs (20 nm, mean diameter) were synthesized using the Turkevich method:[36] $HAuCl_4 \cdot 3H_2O$ aqueous solution (0.7 mg mL^{-1}) was heated to boiling and Na_3-citrate (2 mg mL^{-1}) was added to the boiling solution with vigorous mechanical stirring. After ca. 30 s the solution turned dark-blue and then wine-red. The heating mantle was removed after ca. 10 min; the solution was left to cool with stirring. The calculated concentration (C_{cal}) of the small NP solution (assuming 100% reaction yield) was 4.3×10^{11} NPs/mL. Large Au NPs (63 nm, mean diameter) were prepared using a smaller ratio of Na_3-citrate to $NaAuCl_4 \cdot 2H_2O$, following the procedure of Frens.[37] The boiling solution of $NaAuCl_4 \cdot 2H_2O$ (0.2 mg mL^{-1}) turned dark-blue and then brownish-purple less than 1 min after addition of Na_3-citrate (0.15 mg mL^{-1}). The solution was left to heat for additional 5 min. C_{cal} of the large NP solution was 4×10^{10} NPs/mL.

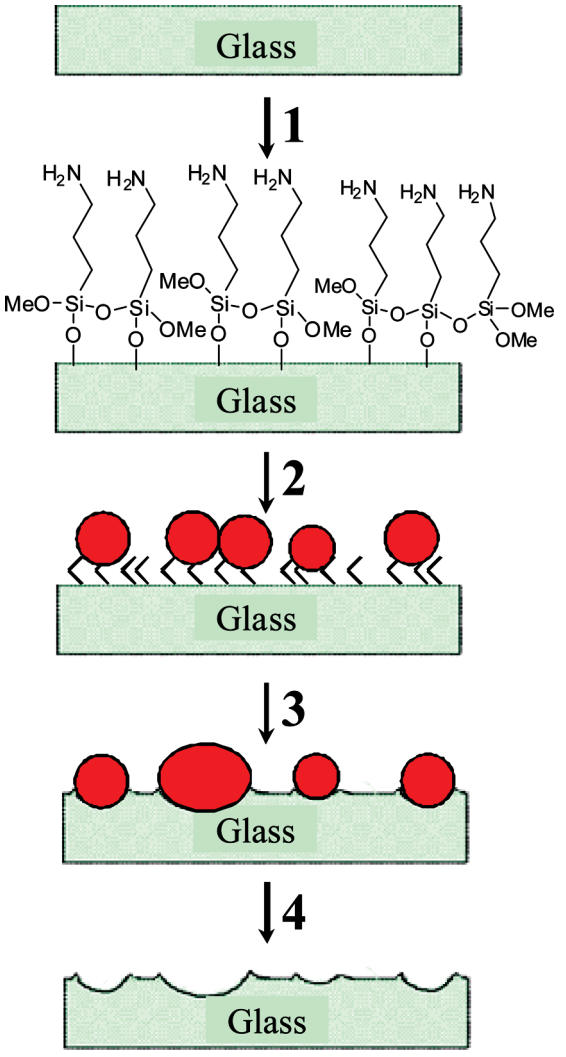

Figure 1. Schematic presentation of Au NP film preparation and dissolution: (1) silanization of the glass substrate; (2) citrate-stabilized Au NP immobilization on the glass; (3) thermal annealing; (4) dissolution of the Au. Sizes of the various components are not to scale.

Preparation of Gold NP Films. The NP films were prepared by generally following the method of Natan and co-workers.[20] Microscope glass cover slides No. 3 (Schott AG borosilicate glass D263T) with a glass transition temperature T_g = 557 °C[38] supplied by Menzel-Gläser, were cut to 22 × 9 mm^2 pieces and cleaned by immersion in freshly prepared hot piranha solution (1:3 H_2O_2:H_2SO_4) for 1 h (***Caution:*** *Piranha solution reacts violently with organic materials and should be handled with extreme care)* followed by rinsing with triply distilled water, rinsing in ethanol three times in an ultrasonic bath (Cole-Parmer 8890), and drying under a steam of nitrogen. After cleaning, the slides were immersed in 2 mM solution of APTS in ethanol for 1.5 h, rinsed in ethanol and dried under a stream of N_2 (step 1 in Figure 1). Immobilization of Au NPs was achieved by immersion of the silanized glass slides in an aqueous solution of citrate-stabilized Au NPs for various times. The following types of films were used: Films of types 1 and 2 were prepared, respectively, by 1 h and overnight immersion in a 10-fold-diluted stock solution of the small NPs. Films of type 3 (full layer) were prepared by 30 min immersion in the original (undiluted) stock solution of the small NPs. Films of type 4 were obtained by overnight

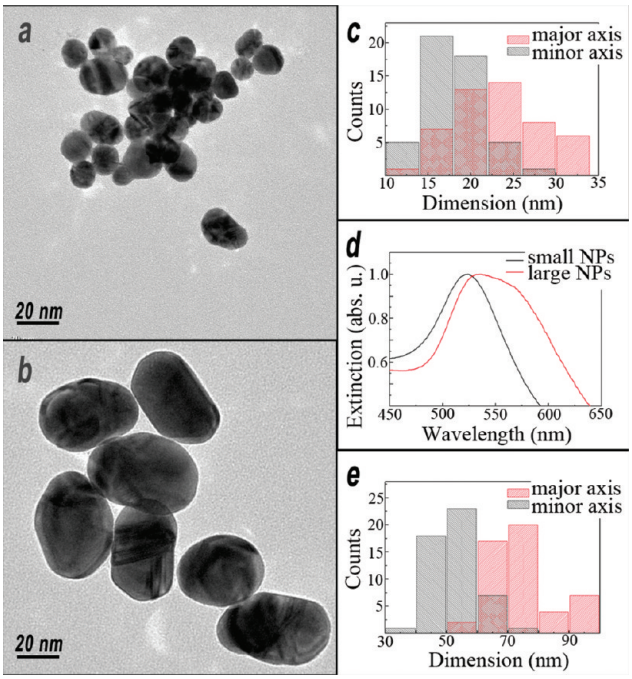

Figure 2. TEM images of (a) small and (b) large citrate-stabilized Au NPs, dried from water. (c, e) Histograms of the major and minor lateral axes of the small and large NPs, respectively. (d) Normalized transmission UV−vis spectra of the Au NPs in aqueous solution.

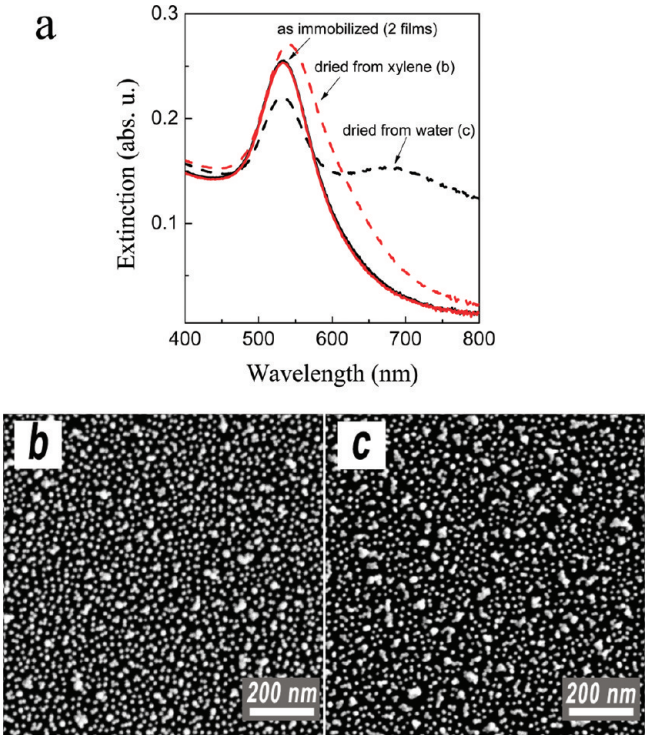

Figure 3. (a) Transmission UV−vis spectra of two samples of citrate-stabilized Au NP films (type 3) immobilized on silanized glass (black and red full lines, overlap) and of the same samples after drying from xylene (red dotted line) and from water (black dashed line). All spectra were measured in water. (b, c): HRSEM images of the films dried from xylene and water, respectively. Image size: 1 × 1 μm^2.

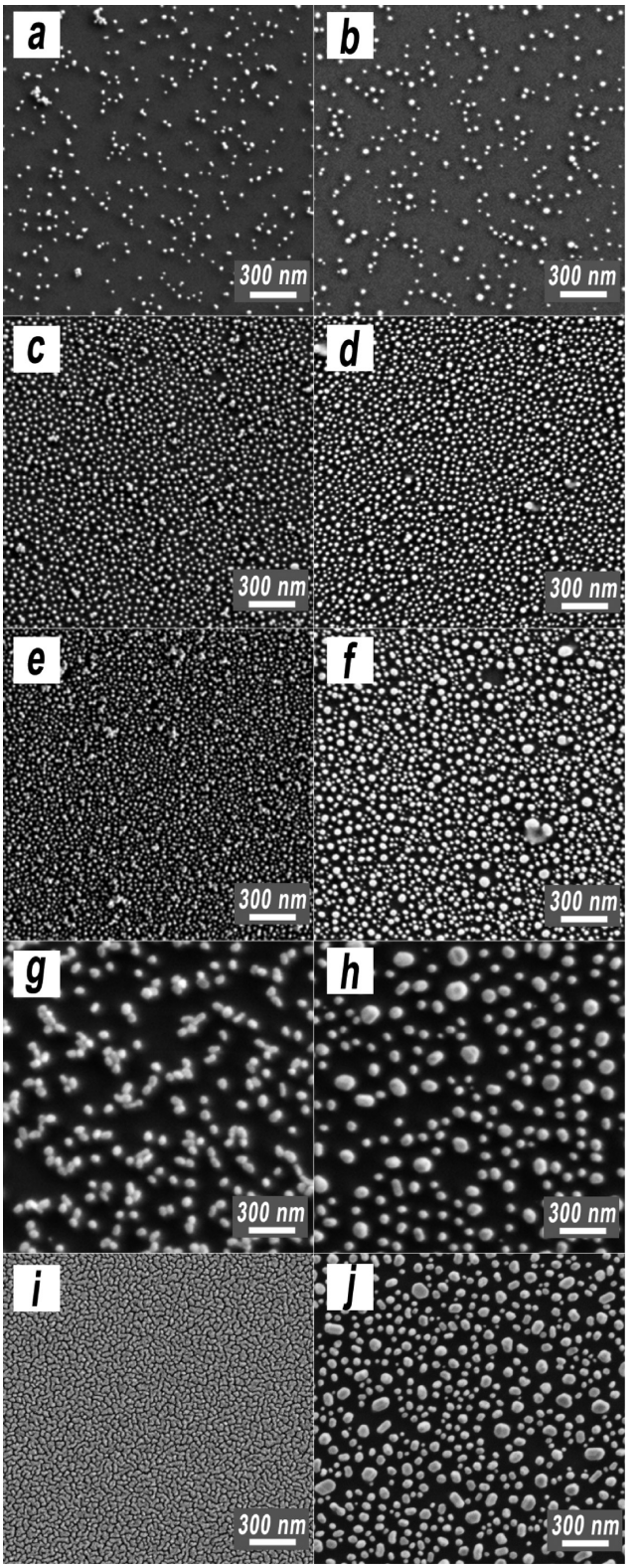

Figure 4. (a−h) HRSEM images of citrate-stabilized Au NP films immobilized on silanized glass, before (left panels) and after (right panels) annealing 10 h at 600 °C, showing films of type (a, b) 1, (c, d) 2, (e, f) 3, and (g, h) 4. Also shown is a 7.5 nm (nominal thickness) Au island film evaporated on glass, (i) before and (j) after annealing 10 h at 600 °C. Image size: 2 × 2 μm^2.

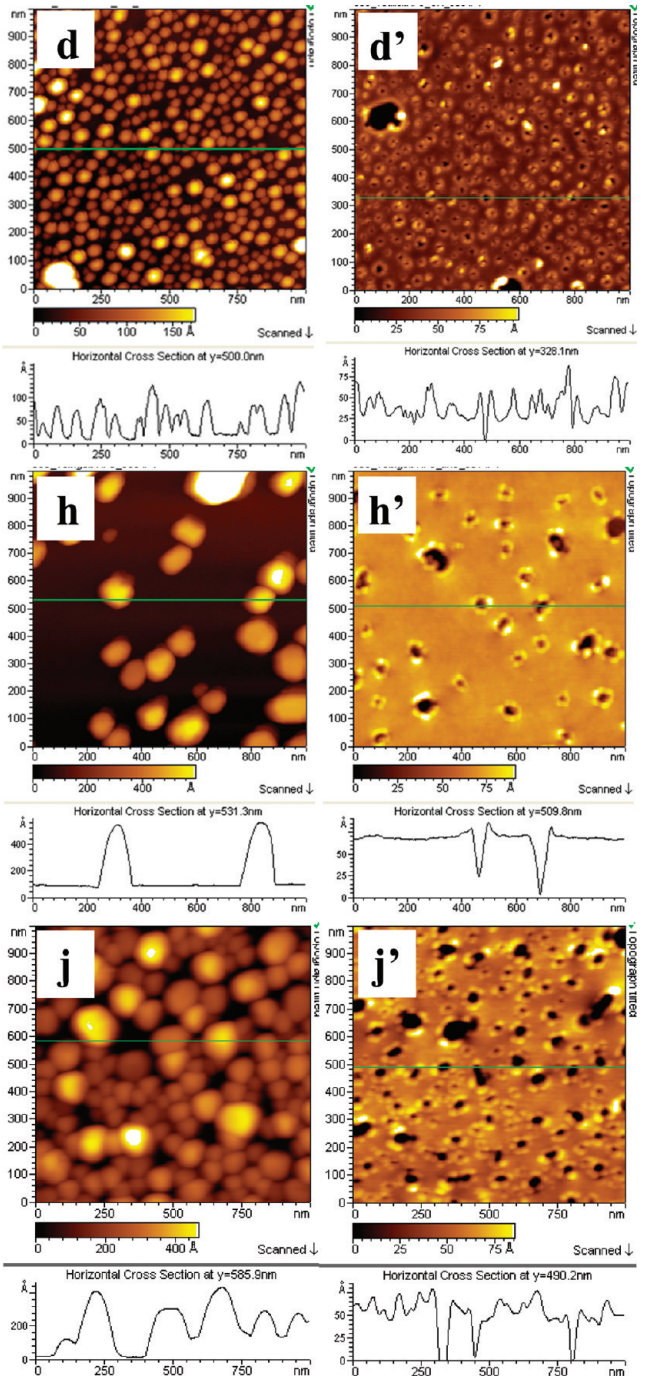

Figure 5. (d, h, j) AFM images ($1 \times 1\ \mu m^2$) of the corresponding samples in Figure 4. (d′, h′, j′) The glass substrates after Au dissolution in iodine tincture. Note the different *z*-scales in different images.

adsorption from a stock solution of the large NPs. After NP immobilization the slides were taken out of the solution without drying, rinsed in xylene, and dried under a N_2 stream (step 2 in Figure 1). Annealing of NP-covered glass slides was carried out in air in an oven (Ney Vulcan 3−550) heated at a rate of 5 °C min^{-1} and held at 600 °C for 10 h. Samples were placed in the oven inside a Kimax Petri dish. The annealed slides were left to cool to room temperature in the oven (step 3 in Figure 1).

Preparation of Gold Island Films. Au island films were deposited according to a procedure described elswere.[25,32] Glass slides were

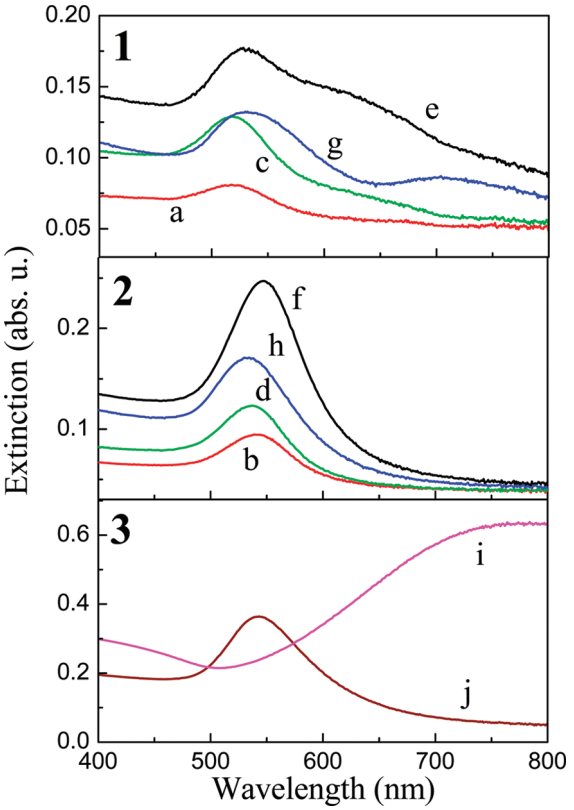

Figure 6. Transmission UV−vis spectra of the samples in Figure 4.

washed in piranha solution for 1 h, rinsed in triply distilled water, rinsed three times in ethanol in an ultrasonic bath, and dried under a stream of nitrogen. 7.5 nm (nominal thickness) Au films were resistively evaporated on the bare glass slides in a cryo-HV evaporator (Key High Vacuum) equipped with a Maxtek TM-100 thickness monitor. Au was evaporated from a tungsten boat at $1-3 \times 10^{-6}$ Torr at a deposition rate of 0.005−0.01 nm s^{-1}. Homogeneous metal deposition was obtained by moderate rotation of the substrate plate. Postdeposition thermal annealing of metal island films was carried out as described above for the Au NP films.

Gold Film Dissolution. Dissolution of nanostructured Au films was carried out by dipping into iodine tincture (3% I_2, 2% KI, 70% ethanol) followed by rinsing with triply distilled water and drying under a N_2 stream (step 4 in Figure 1).

UV−Vis Spectroscopy during Annealing. Figure S1 (Supporting Information) shows the homemade optical tube furnace specially designed for spectroscopic measurements under controlled temperature and environment, enabling performance of transmission UV−vis spectroscopy during high-temperature annealing. The sample was placed in the oven on a quartz tray at room temperature and the heating was turned on. The desired annealing temperature was reached within ca. 15 min. Optical spectra were obtained using a fiber optics based Ocean Optics spectrophotometer (Red Tide USB650). The measurement parameters: integration time, 400 ms; boxcar, 2; scans to average, 5. The baseline was measured at room temperature with the empty quartz tray inserted into the furnace.

Adhesion and Stability Tests. The Au NP adhesion to the glass substrates was evaluated qualitatively using the adhesive tape test: A piece of clear Scotch tape (3M) was pressed against the film and pulled back. Detachment of poorly adhering films was clearly seen with the naked eye. Stability of the optical response was evaluated by comparing transmission UV−vis spectra before and after the following treatments,

Table 1. Statistical Analysis of Gold NP Films Immobilized on Silanized Glass and 7.5 nm Evaporated Au Island Film on Glass, Unannealed (U) and Annealed 10 h at 600 °C (A)

	major axis (nm)		minor axis (nm)		diameter[a] (nm)		aspect ratio (major/minor)		particle surface density $\times 10^{-10}$ (cm^{-2})	
Au film	U	A	U	A	U	A	U	A	U	A
type 1	29 ± 7	28 ± 7	24 ± 5	24 ± 6	26	26	1.21	1.17	1.3	0.79
type 2	19 ± 5	23 ± 7	16 ± 4	19 ± 6	17	21	1.19	1.21	6.0	5.5
type 3	19 ± 7	27 ± 11	15 ± 5	23 ± 10	17	25	1.27	1.17	12	4.3
type 4	69 ± 25	76 ± 26	50 ± 18	62 ± 20	59	69	1.38	1.23	0.72	0.51
island film		47 ± 19		40 ± 15		44		1.18		1.5

[a] The diameter is the average of the mean major and minor axes.

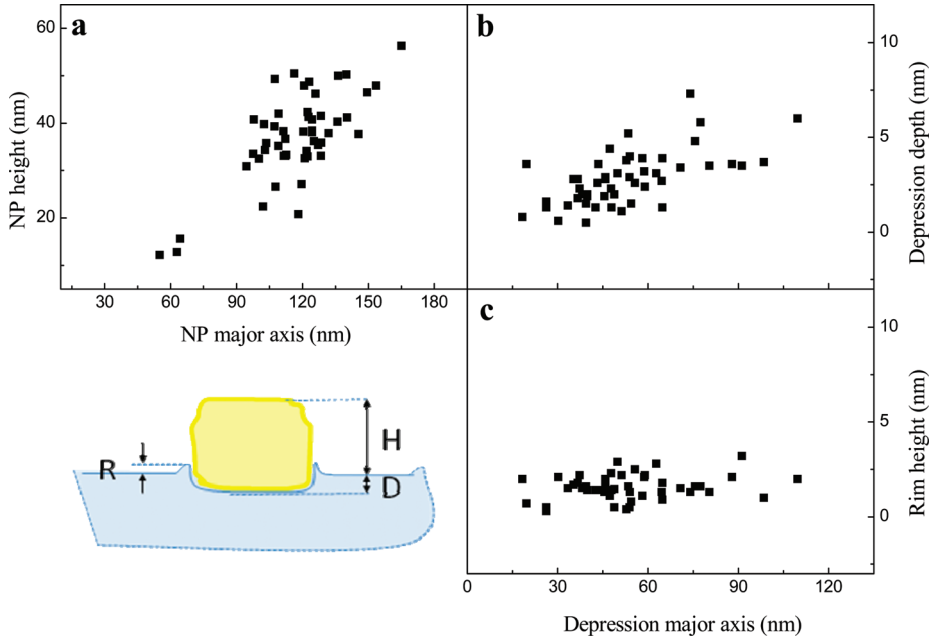

Figure 7. Correlation of (a) NP height, (b) depression depth, and (c) rim height with NP and depression major axes, for Au NP film (type 4) annealed 10 h at 600 °C. All measurements carried out by AFM. Lower left: schematic drawing of a NP embedded in the glass substrate: *H*, NP height above the glass; *D*, depression depth; *R*, rim height.

carried out sequentially: stirring in ethanol for 20 min and drying under a N_2 stream, repeated three times; self-assembly of $C_{18}SH$ from a 1 mM solution in ethanol for 1 h, followed by washing in ethanol and drying; 10 min exposure to UV/ozone (UVOCS model T10 × 10/OES/E) on each side, followed by washing in ethanol and drying; immersion in PBS solution for 20 min followed by washing in water and drying under a N_2 stream.

Au electroless deposition was performed according to a known procedure.[39,40] Annealed Au NP films were immersed in a stirred electroless deposition solution (2.5 mL of hydroxylamine hydrochloride (8 mM), 0.25 mL of chloroauric acid (5 mM), 2.25 mL of water) for various times to deposit Au on the immobilized Au NPs. A fresh solution was used in each deposition.

Refractive Index Sensitivity (RIS) Measurements. The RIS was determined in methanol (n = 1.327), chloroform (n = 1.445), and a 1:1 methanol-chloroform solution (n = 1.391) by recording transmission UV−vis spectra of the various transducers in a quartz cuvette filled with the different solutions.[25] Three data points were sufficient, as the response shows excellent linearity in the measured RI range.[25] The baseline was determined before each measurement using a cuvette with the respective solvent.

Characterization Methods. *UV−Vis Spectroscopy.* Transmission spectra were obtained with a Varian CARY 50 spectrophotometer. The wavelength resolution was 1 nm and the average acquisition time was 0.1 s per point. The slide holder was designed to ensure reproducible position of the sample on the optical axis, with a beam cross-section of ca. 1.5 × 1.5 mm^2. Air was used as baseline for measuring dry samples, whereas for measurements in solution, the baseline was a cuvette filled with the respective solvent.

Atomic force microscopy (AFM) measurements were carried out in air at room temperature (22 ± 1 °C) using a Molecular Imaging (MI) PicoScan instrument operating in the acoustic AC mode. The cantilevers used were NSC35 and NSC36 series of ultrasharp silicon (MikroMasch, Estonia) with a resonant frequency of 90−150 kHz and an average radius of ≤10 nm.

High-resolution scanning electron microscopy (HRSEM) images were obtained with an ULTRA 55 FEG ZEISS high-resolution SEM using the SE detector. The measurements were carried out at an applied voltage of 2 kV and a working distance of 3 mm.

Transmission electron microscopy (TEM) imaging was performed with a Philips CM-120 transmission electron microscope operating at 120 kV, equipped with a CCD camera (2kx2k, Gatan Ultrascan 1000). TEM samples were prepared by placing a drop of the Au NP solution on a copper grid coated with cellulose and carbon and allowing to dry.

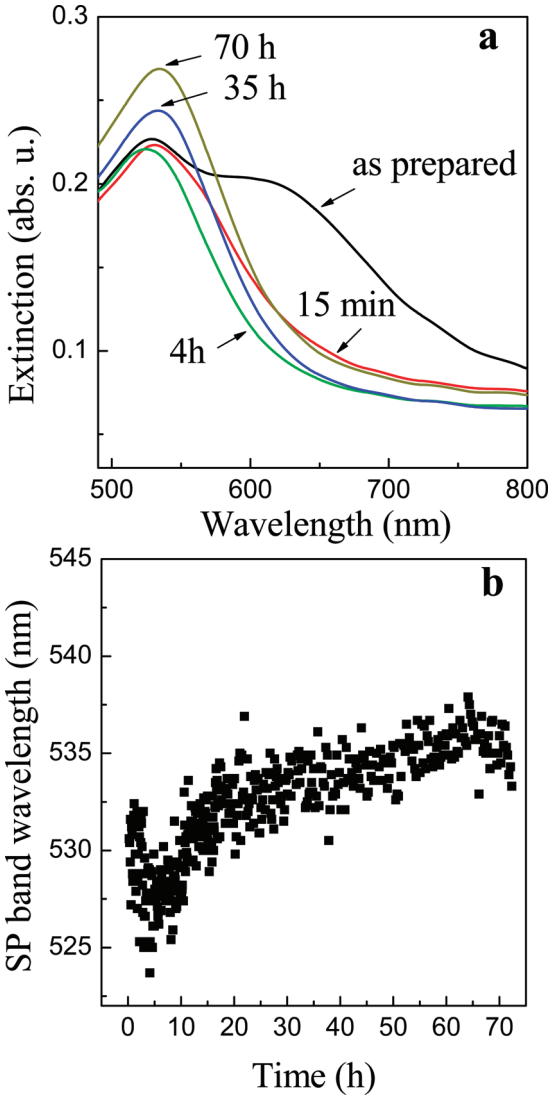

Figure 8. Kinetics of Au NP film (type 3) annealing at 600 °C, measured during the annealing. (a) Transmission UV−vis spectra taken in situ at indicated times. (b) Shift of the wavelength of the SP band maximum during annealing.

RESULTS AND DISCUSSION

Citrate-stabilized Au NPs were characterized by TEM imaging (Figure 2a, b) and transmission UV−vis spectroscopy (Figure 2d). Quantitative determination of the average NP size and distribution was carried out manually on TEM images of 50 particles. Values of the major and minor lateral dimensions of the NPs were analyzed statistically (Figure 2c, e). The small NPs are close to spherical (Figure 2a) with a mean major and minor axes of 23 ± 5 nm and 18 ± 3 nm, respectively. This is expressed in the transmission UV−vis spectrum as a single SP band with a maximum at 523 nm (Figure 2d). The use of a smaller amount of capping agent during preparation leads to particle enlargement and elongation (Figure 2b). The large Au NPs have major and minor axes of 74 ± 11 nm and 53 ± 8 nm, respectively. The transmission UV−vis spectrum shows a SP peak at 534 nm and a shoulder at 563 nm, corresponding to the transverse and longitudinal SP excitations, respectively.

Preparation of NP films by adsorption from a colloid solution and drying frequently results in drying patterns and NP aggregation on the surface,[20] strongly affecting the spectrum. As seen in Figure 3, use of xylene for the final rinse rather than water and drying from the organic solvent (see Experimental Section) enables preservation of the general shape of the SP extinction band. After drying from xylene the spectrum shows a single SP peak generally resembling the spectrum before drying, whereas drying from water leads to the appearance of a second, red-shifted band (Figure 3a). The spectroscopic data are in agreement with the HRSEM images, i.e., drying form xylene results in less aggregation with mostly symmetrical aggregates (Figure 3b), whereas drying from water reveals a considerable number of larger, elongated structures (Figure 3c). Correspondingly, the SP band of the sample dried from water is split to transverse and longitudinal components[41,42] (Figure 3a). Note that all the spectra in Figure 3a (including those of samples after drying) were taken in water to eliminate the effect of the RI of the medium.

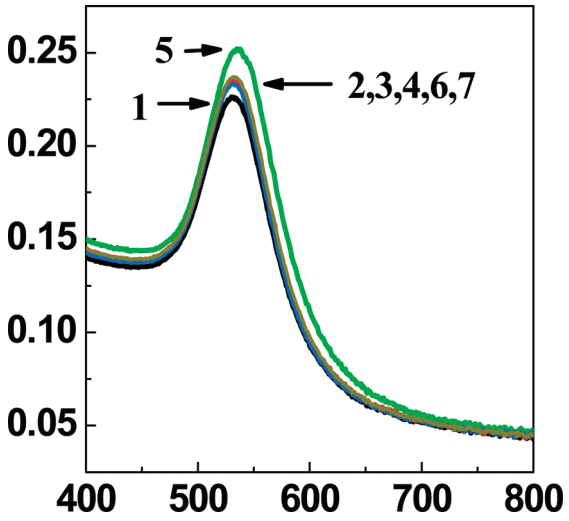

Figure 9. Transmission UV−vis spectra of Au NP film (type 3) annealed 10 h at 600 °C, after the following treatment steps: (1) initial film; (2−4) three consecutive cycles of ethanol wash and drying; (5) self-assembly of a $C_{18}SH$ monolayer + ethanol wash and drying; (6) UV/ozone + ethanol wash and drying; (7) immersion in PBS, followed by washing in water and drying.

The morphology of the Au NP films before and after annealing was characterized by HRSEM (Figure 4) and AFM (Figures 5) imaging. HRSEM images of the unannealed immobilized Au NPs (Figure 4a, c, e, g) are typical of this systems, showing large areas with evenly distributed, isolated Au NPs, as well as NP aggregates, the latter formed mostly during drying when capillary forces displace some Au NPs and induce a certain degree of coalescence. This behavior is especially prominent in films of types 3 and 4 (Figure 4e, g). The respective UV−vis spectra (Figure 6, panel 1) reflect the film morphology, showing aggregate bands increasing from a to g.

Annealing 10 h at 600 °C leads to coalescence of closely spaced NPs and NP aggregates, forming large, symmetric particles, mostly separated by an exclusion zone (Figures 4b, d, f, h and 5d, h). The UV−vis spectra undergo a corresponding transformation, exhibiting a single SP band characteristic of well-separated, symmetric nanostructures (Figure 6, panel 2). The surface coverage by the small NPs increases from 5% (film type 1, Figure 4b) to 21% (film type 2, Figures 4d and 5d) to 24% (film type 3, Figure 4f), whereas the large NPs (film type 4, Figures 4h and 5h) display a 20% surface coverage.

Table 2. Refractive Index Sensitivity (RIS) of Au NP Films Immobilized on Silanized Glass and 7.5 nm Evaporated Au Island Film on Glass, All Annealed 10 h at 600 °C

Au film	SP band wavelength (nm)	RIS_λ (nm/RIU)	RIS_{ext} (abs.u./RIU)	normalized RIS_{ext}[a] × 10^{12} (abs.u. cm^2/RIU)
type 1	541 ± 5	40 ± 6	0.09 ± 0.07	11
type 2	543 ± 5	34 ± 6	0.15 ± 0.04	2.6
type 3	548 ± 6	36 ± 6	0.29 ± 0.11	6.8
type 4	545 ± 3	48 ± 6	0.40 ± 0.21	79
island film	560 ± 2	68 ± 8	0.38 ± 0.02	25

[a] RIS_{ext} is normalized to the NP surface density.

Statistical analysis of Au NP films, as-prepared (unannealed) and annealed 10 h at 600 °C, was performed on HRSEM images (ensembles of 400 NPs in Figure 4) using ImageJ software[43] (Figure S2, Supporting Information, and Table 1). After annealing, the NPs become generally larger and more rounded, attributed to coalescence of adjacent particles. The different values of the average NP size in unannealed films of types 1−3 and the TEM measurements (see above) reflect the relatively large standard deviation as well as the possibility of size-selectivity in the NP binding process under different conditions.[44]

Figures 4i, j and 5j present, for comparison, HRSEM and AFM images of 7.5 nm (nominal thickness) Au island film evaporated on glass, before and after annealing 10 h at 600 °C. The as-prepared Au island film (Figure 4i) shows a near-percolated structure with a network of voids, while the annealing leads to formation of well-separated islands (Figures 4j and 5j) and a corresponding transformation of the UV−vis spectrum (Figure 6, panel 3).[25] The surface coverage of the annealed Au island film is ca. 26%. It should be noted that in our hands the morphology and optical properties of Au island films are more reproducible than those of the NP films.

The morphology of the NP−glass interface before and after annealing was studied by complete dissolution of the Au NPs in iodine tincture. The AFM image of a glass substrate after immobilization of Au NPs, washing, drying and NP dissolution shows a featureless flat surface (not shown), similar to the pristine glass surface. On the other hand, the morphology of the glass substrate after annealing and Au dissolution (Figure 5d′, h′) unveils depressions in the glass similar in spacing to the Au NPs, indicating partial embedding of the annealed NPs in the glass. The NP embedding is analogous to that observed with evaporated Au island films (Figure 5j, j′), shown previously.[25,32]

The process of embedding of Au nanostructures in the glass substrate is controlled by the annealing temperature and time.[25,32] Rapid creation of a glass rim around the islands and slow sinking into the glass (depression depth: 4 ± 3 nm) are observed for the 7.5 nm Au island film upon annealing 10 h at 600 °C (Figure 5j′). For the small NPs evaluation of the depression depth after Au dissolution is complicated (Figure 5d′) because of the small NP lateral dimensions with respect to the AFM tip radius. Correlation of NP height, depression depth and rim height with the NP and depression major axes for 50 NPs/depressions is presented in Figure 7 for the large NPs (film type 4).The mean NP major axis measured by AFM is considerably larger than that of the depressions (Figures 5 and 7a, b), attributed to tip convolution, increasing the measured NP and rim lateral dimensions while decreasing those of the depressions. The average depression depth in the case of film type 4 is 3 ± 1 nm (Figures 5h′ and 7). Figure 7b suggests that the depression depth is correlated to the NP dimensions, similar to annealed evaporated Au islands.[45] The relative depression depth is similar for all NP sizes, i.e., ca. 5% of the NP major axis for 10 h annealing. The glass rim height is nearly independent of the NP size (Figure 7c). The driving force for NP embedding in the softened glass is most likely capillary forces at the glass−NP−air three-phase interface.[32]

The kinetics of Au NP film annealing were studied by in situ measurements of transmission UV−vis spectra during the annealing process using a special oven (see Experimental Section). Transmission spectra of a NP film (type 3) were recorded in situ at different times during annealing at 600 °C (Figure 8). The main structural modification of the NPs, i.e., coalescence of adjacent NPs, occurs within ca. 15 min (during oven heating), seen as convergence of the two SP peaks to a single wide band. The following ca. 4 h display narrowing of the extinction band, i.e., diminution of the tail and an accompanying blue-shift of the SP maximum (Figure 8a). The SP band wavelength reaches a minimum at ca. 4 h annealing, after which a steady red-shift dominates (Figure 8b) together with increase of the SP band intensity (Figure 8a).

Although the major NP structural transformation occurs in the first minutes of annealing, as in the case of evaporated Au island films,[32] the change of the band shape and blue-shift of the SP maximum in the first few hours of annealing suggest additional (possibly small) NP reshaping. The subsequent gradual SP red-shift and intensity increase are attributed to the Au NP embedding in the glass substrate, as expected from the higher RI of the glass (1.52) compared to air (1.00).

Annealing at temperatures close to T_g of the glass substrate (T_g = 557 °C) results in significant improvement of the adhesion between the Au NP film and the substrate. Unannealed Au NP films are readily removed in the adhesive tape test, whereas all films annealed 10 h at 600 °C pass the adhesive tape test successfully and remain intact, as in the case of similarly annealed Au island films.[32]

The stability of the optical response of the annealed Au NP films was evaluated by subjecting a film of type 3, annealed 10 h at 600 °C, to solvent immersion followed by drying. The first cycle of washing in ethanol and drying causes an initial change of the spectrum (Figure 9, line 2), which remains unchanged after subsequent cycles of washing and drying (Figure 9, lines 3, 4), indicating a stable film morphology. Self-assembly of $C_{18}SH$ on the partially embedded Au NPs leads to increase in the extinction and a SP red-shift (Figure 9, line 5), indicative of the self-assembled monolayer (SAM) formation. Removal of the SAM by UV-ozone treatment and subsequent ethanol wash[46] nearly perfectly restores the transmission spectrum (Figure 9, line 6), confirming the stability of the NP film morphology. The spectrum remains intact after washing the film in PBS solution and drying (Figure 9, line 7), a crucial medium for biological

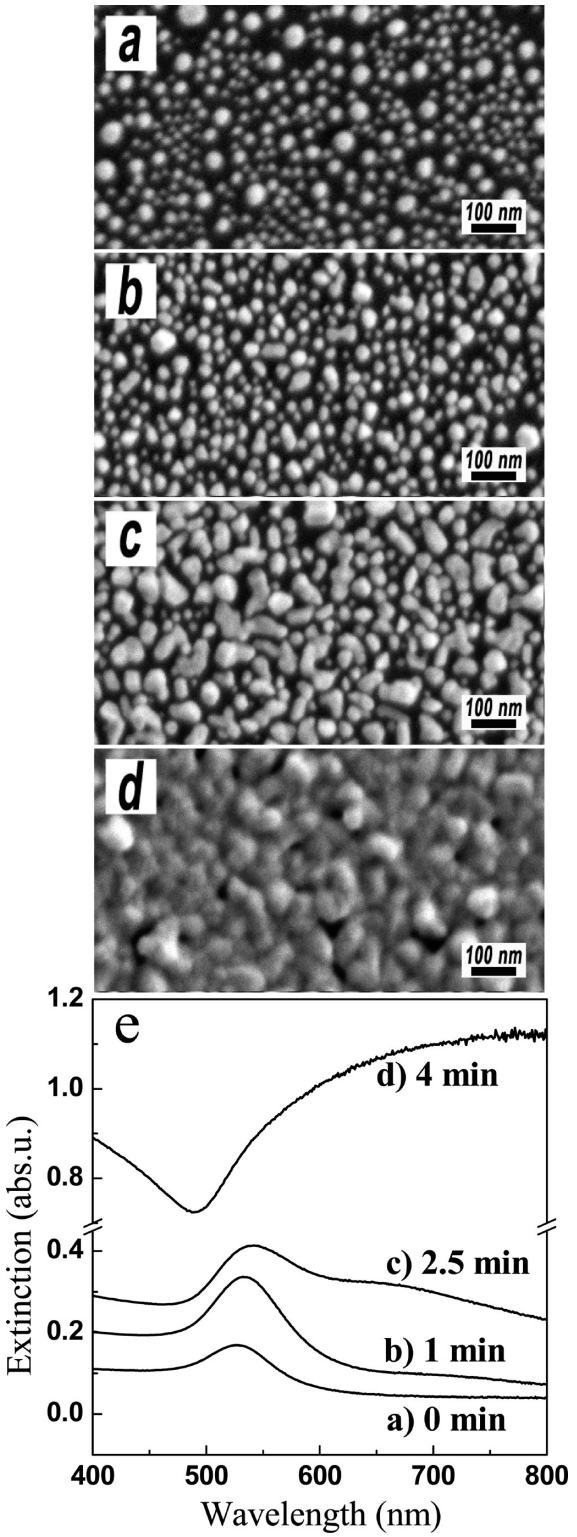

Figure 10. HRSEM images of Au NP films (type 3) annealed 10 h at 600 °C, shown after Au electroless deposition for (a) 0, (b) 1, (c) 2.5, and (d) 4 min. (e): corresponding transmission UV−vis spectra.

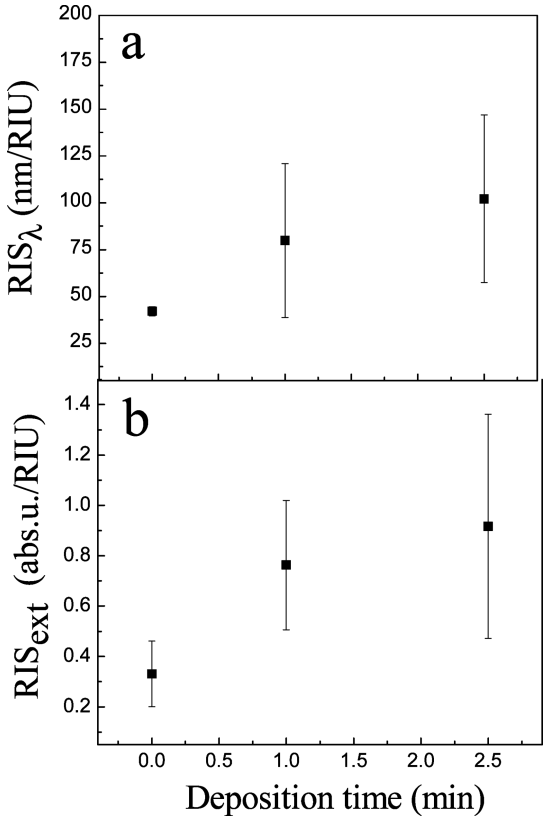

Figure 11. (a) RIS$_\lambda$ and (b) RIS$_{ext}$ of Au NP films (type 3) annealed 10 h at 600 °C, before and after Au electroless deposition for indicated times.

applications, presenting particularly harsh conditions for the stability of Au nanoparticulate films.[31] On the other hand, unannealed Au NP films prepared by drying from water or from xylene show unsatisfactory stability when subjected to the same conditions (see Figures S3 and S4 in the Supporting Information).

The bulk refractive index sensitivity (RIS) of annealed NP films was evaluated as RIS$_\lambda$ (for SP wavelength shift) and RIS$_{ext}$ (for SP peak intensity change) by recording optical spectra of NP film transducers in a series of solvents in the RI range 1.327−1.445, where the response is linear with RI;[25] the values are reported in Table 2. Films of types 1−3 (small NPs) show close values of the RIS$_\lambda$ in the range 34−40 nm/RIU without clear dependence on the particle surface density. On the other hand, the RIS$_{ext}$ increases with the increase in Au NP density on the surface (RIS$_{ext}$ ranges from 0.09 to 0.29 abs.u./RIU).

We have previously shown that analysis of trends in the RIS$_\lambda$ vs RIS$_{ext}$ values requires normalization of the RIS$_{ext}$ to the NP surface concentration, as its value is directly related to the number of NPs sampled.[47] The normalized RIS$_{ext}$ values for films of types 1−3 given in Table 2 (2.6×10^{-12} to 11×10^{-12} abs.u.·cm^2/RIU) show the same qualitative behavior as the RIS$_\lambda$ values, reflecting the trend in the average NP diameter. Type 4 film and the evaporated island film, both comprising larger particles, show higher RIS values.

The RIS of NP films is closely related to the NP size and shape.[48,49] In an attempt to enhance the RIS of embedded NP films by modifying the film morphology, electroless deposition of Au on the NPs was applied.[19,39,40,50−54] Figure 10 presents HRSEM images of Au NP films (type 3) annealed 10 h at 600 °C, before and after 1, 2.5, and 4 min electroless deposition of Au. The NPs gradually increase in size and become irregularly shaped with deposition time (Figure 10b, c), until a percolated

film is attained after ca. 4 min deposition (Figure 10d). The transmission spectra (Figure 10e) reflect the morphology transformation, i.e., isolated NPs (line a), larger NPs with some elongated particles (line b), mostly elongated, wormlike nanostructures (line c), and a continuous Au film (line d). The respective RIS values are presented in Figure 11. Despite the rather large standard deviation of the RIS values after Au deposition, an increase of up to a factor of 3 is achieved after 2.5 min electroless deposition, attributed to the change in size and shape of the NPs.

The system stability is largely maintained after the electroless deposition. Whereas the optical response of the pristine embedded NP film stabilizes after one cycle of ethanol wash and drying (Figure 9), following Au electroless deposition the response becomes stable after 3−4 such cycles and remains stable thereafter.

CONCLUSIONS

Au nanoparticle (NP) films prepared by electrostatic binding of citrate-stabilized NPs on aminosilane-terminated glass substrates show improved NP distribution and reduced aggregation when dried from xylene rather than from water. Postdeposition annealing of the Au NP films at 600 °C, i.e., slightly above the substrate glass transition temperature (T_g = 557 °C), promotes morphology transformation and gradual NP embedding in the glass substrate accompanied by formation of a glass rim around the NPs. Transmission UV−vis spectra measured in situ during the annealing provided information on the different stages of the thermally induced structure evolution, including initial, relatively fast morphological change; slow additional reshaping and initial embedding; and gradually increasing embedding in the glass. Transducers comprising partially embedded Au NPs are exceedingly stable toward immersion in solvents, drying, and formation of a thiol SAM, and pass successfully the adhesive tape test. The superior adhesion is attributed to embedding of the NP bottom part in the glass and rim formation.

The bulk refractive index sensitivity (RIS) of thermally embedded Au NP films is 34−48 nm/RIU (RIS_λ) and 0.1−0.4 abs.u./RIU (RIS_{ext}). The RIS of the transducers was increased up to 3-fold by Au electroless deposition on the partially embedded Au NPs, providing a reasonably sensitive and stable LSPR transducer platform.

ASSOCIATED CONTENT

Supporting Information. Additional figures (PDF). This material is available free of charge via the Internet at http://pubs.acs.org.

AUTHOR INFORMATION

Corresponding Author

*E-mail: alexander.vaskevich@weizmann.ac.il (A.V.); israel.rubinstein@weizmann.ac.il (I.R.).

ACKNOWLEDGMENT

Support of this work by the Israel Science Foundation, Grant 672/07, is gratefully acknowledged. This research is made possible in part by the historic generosity of the Harold Perlman family. The electron microscopy studies were conducted at the Irving and Cherna Moskowitz Center for Nano and Bio-Nano Imaging, Weizmann Institute of Science.

REFERENCES

(1) Feldheim, D. L.; Foss, C. A.; Jr. *Metal Nanoparticles: Synthesis, Characterization, and Applications*;Marcel Dekker: New York, 2002.
(2) Hutter, E.; Fendler, J. H. *Adv. Mater.* **2004**, *16*, 1685–1706.
(3) Stewart, M. E.; Anderton, C. R.; Thompson, L. B.; Maria, J.; Gray, S. K.; Rogers, J. A.; Nuzzo, R. G. *Chem. Rev.* **2008**, *108*, 494–521.
(4) Vaskevich, A.; Rubinstein, I. . In *Handbook of Biosensors and Biochips*; Marks, R., Cullen, D., Lowe, C., Weetall, H. H., Karube, I., Eds.; Wiley: Chichester, U.K., 2007; Vol. 1.
(5) Kalyuzhny, G.; Vaskevich, A.; Ashkenazy, G.; Shanzer, A.; Rubinstein, I. *J. Phys. Chem. B* **2000**, *104*, 8238–8244.
(6) Gluodenis, M.; Manley, C.; Foss, C. A. *Anal. Chem.* **1999**, *71*, 4554–4558.
(7) Kalyuzhny, G.; Schneeweiss, M. A.; Shanzer, A.; Vaskevich, A.; Rubinstein, I. *J. Am. Chem. Soc.* **2001**, *123*, 3177–3178.
(8) Kalyuzhny, G.; Vaskevich, A.; Schneeweiss, M. A.; Rubinstein, I. *Chem. - Eur. J.* **2002**, *8*, 3850–3857.
(9) Meriaudeau, F.; Downey, T. R.; Passian, A.; Wig, A.; Ferrell, T. L. *Appl. Opt.* **1998**, *37*, 8030–8037.
(10) Doron-Mor, I.; Barkay, Z.; Filip-Granit, N.; Vaskevich, A.; Rubinstein, I. *Chem. Meter.* **2004**, *16*, 3476–3483.
(11) Haes, A. J.; Van Duyne, R. P. *J. Am. Chem. Soc.* **2002**, *124*, 10596–10604.
(12) Haes, A. J.; Zou, S. L.; Schatz, G. C.; Van Duyne, R. P. *J. Phys. Chem. B* **2004**, *108*, 6961–6968.
(13) Jensen, T. R.; Duval, M. L.; Kelly, K. L.; Lazarides, A. A.; Schatz, G. C.; Van Duyne, R. P. *J. Phys. Chem. B* **1999**, *103*, 9846–9853.
(14) Malinsky, M. D.; Kelly, K. L.; Schatz, G. C.; Van Duyne, R. P. *J. Am. Chem. Soc.* **2001**, *123*, 1471–1482.
(15) Takei, H. In . In *Microfluidic Devices and Systems*; Frazier, A. B., Chong, H. A., Eds.; SPIE: Bellingham, WA, 1998; Vol. 3515, pp 278−283.
(16) Nath, N.; Chilkoti, A. *Anal. Chem.* **2002**, *74*, 504–509.
(17) Nath, N.; Chilkoti, A. *Anal. Chem.* **2004**, *76*, 5370–5378.
(18) Okamoto, T.; Yamaguchi, I.; Kobayashi, T. *Opt. Lett.* **2000**, *25*, 372–374.
(19) Frederix, F.; Friedt, J.-M.; Choi, K.-H.; Laureyn, W.; Campitelli, A.; Mondelaers, D.; Maes, G.; Borghs, G. *Anal. Chem.* **2003**, *75*, 6894–6900.
(20) Grabar, K. C.; Freeman, R. G.; Hommer, M. B.; Natan, M. J. *Anal. Chem.* **1995**, *67*, 735–743.
(21) Ye, J.; Bonroy, K.; Nelis, D.; Frederix, F.; D'Haen, J.; Maes, G.; Borghs, G. *Colloids Surf., A* **2008**, *321*, 313–317.
(22) Ishikawa, H.; Kimura, K. *Nanostruct. Mater.* **1997**, *9*, 555–558.
(23) Pilyankevich, A. N.; Melnikova, V. A. *Thin Solid Films* **1976**, *37*, L25–L28.
(24) Doron-Mor, I.; Cohen, H.; Barkay, Z.; Shanzer, A.; Vaskevich, A.; Rubinstein, I. *Chem. - Eur. J.* **2005**, *11*, 5555–5562.
(25) Karakouz, T.; Holder, D.; Goomanovsky, M.; Vaskevich, A.; Rubinstein, I. *Chem. Mater.* **2009**, *21*, 5875–5885.
(26) Doron, A.; Katz, E.; Willner, I. *Langmuir* **1995**, *11*, 1313–1317.
(27) Zhang, X.; Zhao, J.; Whitney, A. V.; Elam, J. W.; Van Duyne, R. P. *J. Am. Chem. Soc.* **2006**, *128*, 10304–10309.
(28) Scholes, F. H.; Bendavid, A.; Glenn, F. L.; Critchley, M.; Davis, T. J.; Sexton, B. A. *J. Raman Spectrosc.* **2008**, *39*, 673–678.
(29) Banholzer, M. J.; Harris, N.; Millstone, J. E.; Schatz, G. C.; Mirkin, C. A. *J. Phys. Chem. C* **2010**, *114*, 7521–7526.
(30) Im, H.; Lindquist, N. C.; Lesuffleur, A.; Oh, S.-H. *ACS Nano* **2010**, *4*, 947–954.
(31) Ruach-Nir, I.; Bendikov, T. A.; Doron-Mor, I.; Barkay, Z.; Vaskevich, A.; Rubinstein, I. *J. Am. Chem. Soc.* **2007**, *129*, 84–92.
(32) Karakouz, T.; Tesler, A. B.; Bendikov, T. A.; Vaskevich, A.; Rubinstein, I. *Adv. Mater.* **2008**, *20*, 3893–3899.

(33) Natan, M. J.; Reiss, B. D.; Keefe, M. H. PCT US00/32854 (Dec. 04, 2000) and WO 01/40132 (June 7, 2001).
(34) Vakarelski, I. U.; Maenosono, R.; Kwek, J. W.; Higashitani, K. *Colloid Surf., A* **2009**, *340*, 193–198.
(35) Block, B. P. . In *Inorganic Syntheses*; Bailar, J. C., Jr., Ed.; McGraw-Hill: New York, 1953; Vol. 4, pp 14−17.
(36) Turkevich, J.; Stevenson, P. C.; Hillier, J. *Discuss. Faraday Soc.* **1951**, *No. 11*, 55–75.
(37) Frens, G. *Nat. Phys. Sci.* **1973**, *241*, 20–22.
(38) The value of T_g was provided by SCHOTT AG, Mainz.
(39) Brown, K. R.; Natan, M. J. *Langmuir* **1998**, *14*, 726–728.
(40) Brown, K. R.; Lyon, L. A.; Fox, A. P.; Reiss, B. D.; Natan, M. J. *Chem. Mater.* **2000**, *12*, 314–323.
(41) Nikoobakht, B.; El-Sayed, M. A. *Chem. Mater.* **2003**, *15*, 1957–1962.
(42) Murphy, C. J.; Gole, A. M.; Hunyadi, S. E.; Stone, J. W.; Sisco, P. N.; Alkilany, A.; Kinard, B. E.; Hankins, P. *Chem. Commun.* **2008**, 544–557.
(43) The NP major and minor axes and surface coverage (area fraction) were calculated using ImageJ image processing software (ImageJ 1.29x, Wayne Rasband, National Institute of Health, USA; http://rsb.info.nih.gov/ij). Identification of the Au NPs by the software was done by adjustment of the image intensity threshold.
(44) Hanarp, P.; Sutherland, D. S.; Gold, J.; Kasemo, B. *J. Colloid Interface Sci.* **2001**, *241*, 26–31.
(45) Karakouz, T.; Vaskevich, A.; Rubinstein, I., *Kinetics of High Temperature Annealing*; Weizmann Institute of Science: Rehovot, Israel, 2010.
(46) Ron, H.; Matlis, S.; Rubinstein, I. *Langmuir* **1998**, *14*, 1116–1121.
(47) Kedem, O.; Tesler, A. B.; Vaskevich, A.; Rubinstein, I. *ACS Nano* **2011**, *5*, 748–760.
(48) Chen, H. J.; Kou, X. S.; Yang, Z.; Ni, W. H.; Wang, J. F. *Langmuir* **2008**, *24*, 5233–5237.
(49) Lee, K. S.; El-Sayed, M. A. *J. Phys. Chem. B* **2006**, *110*, 19220–19225.
(50) Musick, M. D.; Pena, D. J.; Botsko, S. L.; McEvoy, T. M.; Richardson, J. N.; Natan, M. J. *Langmuir* **1999**, *15*, 844–850.
(51) Meltzer, S.; Resch, R.; Koel, B. E.; Thompson, M. E.; Madhukar, A.; Requicha, A. A. G.; Will, P. *Langmuir* **2001**, *17*, 1713–1718.
(52) Sukhov, V. M.; Dement'eva, O. V.; Kartseva, M. E.; Rudoy, V. M.; Ogarev, V. A. *Colloid J.* **2004**, *66*, 482–488.
(53) Ha, D. H.; Kim, S.; Yun, Y. J.; Park, H. J.; Yun, W. S.; Song, J. H. *Nanotechnology* **2009**, 20.
(54) Ma, Z. F.; Sui, S. F. *Angew. Chem., Int. Ed.* **2002**, *41*, 2176–2179.